Laboratory Studies of OBrO

Gary Knight,† A. R. Ravishankara,‡ and James B. Burkholder*

Aeronomy Laboratory, National Oceanic and Atmospheric Administration, 325 Broadway, Boulder, Colorado 80303

Received: June 21, 2000; In Final Form: September 26, 2000

UV/vis absorption cross sections for gas phase OBrO at room temperature were measured using a fast gas flow absorption cell and a diode array spectrometer. The OBrO concentration was determined by chemical titration $NO + OBrO \rightarrow NO_2 + BrO$ (1) with quantitative measurement of the NO_2 product by UV absorption. The cross section at the peak of the $C\ ^2A_2$ (710) ← $X\ ^2B_1$ (000) transition, ∼491 nm, was determined to be $(1.8 \pm 0.5) \times 10^{-17}$ cm^2 molecule^{-1}. During these measurements another gas phase UV absorber was observed to originate from the OBrO source. The possible identity of this species and its influence on the OBrO absorption cross section determination are discussed.

Introduction

The importance of bromine chemistry, in particular its role in the catalytic destruction of stratospheric ozone, is now widely accepted.[1,2] The reactive bromine species in the atmosphere are Br and BrO while HOBr and $BrONO_2$ act as temporary reservoir species. Other bromine oxides have received consideration but have been generally thought to play only a minor role in atmospheric chemistry.[3−10]

Interest in OBrO has recently risen following its reported detection in the nighttime mid-latitude stratosphere[11] by UV/vis absorption measurements made using stellar occultation from a balloon-borne instrument. Using the OBrO spectrum from the literature[6] and assuming absorption cross sections similar to that for OClO, Renard et al. derived OBrO mixing ratios of 20 to 25 pptv. A OBrO mixing ratio this large would significantly alter our current understanding of nighttime atmospheric bromine chemistry. Chipperfield et al.[12] have examined a number of the possible stratospheric sources of OBrO in a modeling study but were unable to rationalize such high OBrO mixing ratios. Erle et al.[13] have since reported an upper limit for the OBrO stratospheric mixing ratio of 7.7 pptv. The source of OBrO in the stratosphere remains a mystery.

In this paper, we report measurements of UV/vis absorption cross sections of OBrO. The OBrO concentration was determined by chemical titration

$$NO + OBrO \rightarrow NO_2 + BrO \qquad (1)$$

and the quantitative measurement of the NO_2 by UV absorption. During these measurements another gas phase UV absorber was observed to originate from the OBrO source. The possible identity of this species and its influence on the OBrO cross section determination are discussed.

Experimental Section

Gas phase OBrO has been observed via UV/vis absorption,[6−8] mass spectrometry,[3−5] infrared absorption,[7,14] and rotational spectroscopy.[15] In these experiments, relatively low concentrations of OBrO were produced in situ using discharge flow[3−5] and photochemical techniques[6,8] normally used to produce BrO radicals. A number of these studies also demonstrated that the reaction products of the discharge flow could be condensed ($T < 235$ K) and then evaporated at higher temperatures to yield gas phase OBrO in greater amounts. In each of these studies, the source chemistry of OBrO was not well characterized.

In this study, we have employed the technique used by Li[4,5] of collecting the products of a Br_2/O_2/He discharge flow in a cold trap followed by evaporation at warmer temperatures as a gas phase source of OBrO. OBrO concentrations were determined using chemical titration, reaction 1, where $k_1 = 1.77 \times 10^{-12}$ cm^3 molecule^{-1} s^{-1} at 298 K.[5]

The experimental apparatus consisted of a diode array spectrometer system, combination flow tube/absorption cell, and the OBrO source. The diode array spectrometer system consisted of a 0.5 m spectrometer with a 1024-element diode array detector and a 30 W D_2 lamp light source. Most spectral measurements were made with a 150 grooves/mm holographic grating (335 nm bandwidth) setup to cover the wavelength range 200−535 nm. Typical detector exposure times were ∼0.2 s and spectra were recorded by coadding 20 scans. Reference OBrO spectra were recorded using a Pyrex filter to eliminate second-order light. Spectra recorded during the cross section experiments did not use optical filters. However, test measurements showed that the contribution of second-order light to be within the noise level except, at wavelengths greater than 520 nm.

Absorption spectra were determined by first measuring the lamp spectrum, I_0, while flushing the cell with He. The sample flow was then introduced into the flow tube/absorption cell and spectra, I, were recorded. Absorption spectra were calculated via $A = -\ln(I/I_0)$. Spectral subtractions of Br_2, BrO, and NO_2 were made using measured reference spectra and literature cross sections.[16−18]

The flow tube/absorption cell consisted of a jacketed glass tube (3 cm i.d.) with purged quartz windows. The nominal path length (gas inlet to vacuum outlet) of the absorption cell was 85 cm. The temperature of the cell was maintained by circulating fluids from a temperature regulated reservoir through the cell jacket. A 6 mm o.d. glass movable injector was inserted from

* Address correspondence to this author at NOAA, R/AL2, 325 Broadway, Boulder, CO 80305-3338. E-mail: Burk@al.noaa.gov.
† Also associated with CIRES, University of Colorado, Boulder, CO 80309.
‡ Also associated with Department of Chemistry and Biochemistry, University of Colorado, Boulder, CO 80309.

10.1021/jp002226u CCC: $19.00
Published on Web 10/26/2000

the upstream end of the cell and ran along the bottom of the cell so as not to block the probe beam.

OBrO Source. The effluent of a microwave discharge of a dilute Br_2/O_2 in He mixture was passed through an U-shaped glass trap (16 mm o.d.) before entering the absorption cell. The temperature of the trap was maintained at 235−240 K while samples were being collected. The temperature of the trap was controlled by submersion in a cooled methanol bath in a wide mouth Dewar. The source was operated under fast flow conditions with a pressure of 1.7 Torr and He flow of ∼20 STP $cm^3\ s^{-1}$. The linear gas flow velocity through the trap was ∼12 000 cm s^{-1} (0.002 s residence time) and in the absorption cell it was about 1250 cm s^{-1}. The Br_2 and O_2 flows were optimized by monitoring the BrO radical absorption signal while the U-trap was at room temperature. The maximum BrO signal yielded the most efficient production of condensed material when the trap was cooled. No BrO absorption was detected with the trap cooled. The Br_2 and O_2 concentrations were about 1×10^{14} and 4×10^{14} molecules cm^{-3}, respectively. As observed by Li,[4] we also found that higher Br_2 concentrations reduced the condensed material production. We also observed that passing Br_2/O_2 together through the discharge was more efficient than the reaction

$$O + Br_2 \rightarrow BrO + Br \quad (2)$$

or

$$Br + O_3 \rightarrow BrO + O_2 \quad (3)$$

in producing the condensed material.

A sample collection time of 30 min to 1 h yielded sufficient material for the cross section determination experiments. Although not uniform, we observed sample condensation throughout the entire cold region of the trap. **Warning:** Collecting samples for longer times was attempted but resulted in explosive decomposition of the sample when warmed, as described below. Following the sample collection, the discharge was turned off and the Br_2/O_2 flow stopped. The condensed sample (at ∼240 K) was then flushed with the He flow for 1−2 h. Initially, the sample was a combination of red-brown, yellow, and white. After flushing, the sample took on a more uniform yellow-brown color with small sections of white near the trap inlet.

OBrO was introduced into the UV absorption cell by warming the condensate to 273 K while flushing He through the trap. The OBrO absorption signals were relatively small, $A < 0.003$. Other trap temperatures also yielded OBrO in the gas phase. However, at lower temperatures the gas phase OBrO was too small for accurate absorption measurements. At sample temperatures near and above room temperature the sample showed signs of decomposition as described in the Results and Discussion section. Flowing O atoms through the sample trap ($T =$ 273 K) was found to enchance the gas phase OBrO concentration by as much as a factor of 10. Measurements made with the O atom discharge on and off were used in the cross section determination. Flowing Br atoms, O_2, or O_3 through the sample trap had no affect on the absorption spectra or intensities.

Materials. He (UHP, 99.9995%) was used as the carrier gas after passage through a molecular sieve trap at liquid nitrogen temperature. O_2 (UHP, 99.9995%) was used as supplied. Bromine was purified by repeated freeze−pump−thaw cycles and stored under vacuum. NO (C.P. grade) was purified by passage through a silica gel trap at dry ice temperature. NO_2 was prepared and handled as described by Gierczak et al.[18] O_3 was prepared using standard methods. Gas flows were measured using calibrated electronic flow meters. Pressure was measured with a 10 Torr capacitance manometer.

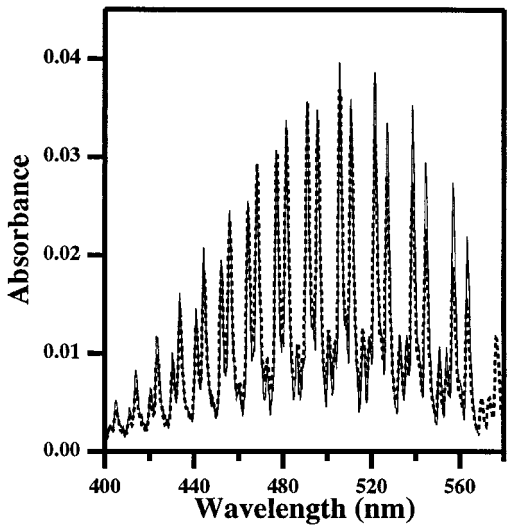

Figure 1. Absorption spectrum of OBrO recorded at 0.66 (solid line) and 1.28 nm (dashed line) resolution. The spectra are normalized at the peak of the C $^2A_2$ (710) ← X $^2B_1$ (000) band.

Results and Discussion

Resolution Dependence of the OBrO Absorption Spectrum. Figure 1 shows OBrO UV/vis absorption spectra recorded in this work at spectral resolutions of 0.66 nm (300 grooves/mm grating) and 1.28 nm (150 grooves/mm grating). Resolution was measured as the fwhm of the 296 nm Hg line. OBrO was produced in the absorption cell using an O atom flow through the source trap. The spectra were normalized to the peak of the (710 ← 000) transition, 491 nm, to enable direct comparison. Our absorption spectra are in good agreement with those previously reported by Rattigan et al.[6] (2.5 and 0.6 nm resolution) and Miller et al.[7] (estimated to be 1 nm resolution). The absorption features at wavelengths shorter than 490 nm are relatively insensitive to our modest change in spectral resolution. However, the bands to longer wavelengths display significant decreases in peak intensity at lower resolution, increasing with increasing wavelength. We attribute these observations to an increase in the unresolved rotational structure with increasing wavelength. Higher resolution spectral measurements are needed to confirm this hypothesis.

The atmospheric measurements of Renard et al.[11] and Erle et al.[13] employed spectral resolutions of 0.7 and 1.2 nm, respectively. Therefore, the cross section measurements derived in this work can be applied directly in their data analysis. However, higher resolution atmospheric measurements especially in the long-wavelength region of the OBrO spectrum may provide improved detection of OBrO.

Spectral Analysis. Absorption spectra recorded under fast flow conditions using the OBrO source at 273 K, with and without the O atom discharge, are shown in Figure 2. The OBrO spectrum between 400 and 535 nm is easily identifiable in both spectra. However, there are several other absorption features between 200 and 400 nm. The vibrational band structure between 300 and 350 nm is due to BrO.[17] However, part of the continuous features lying below the structured BrO spectrum and to shorter wavelengths have not been reported in previous UV absorption studies of OBrO.[6,7] The discharge off spectrum also contains a contribution due to Br_2O. Br_2O is identified by

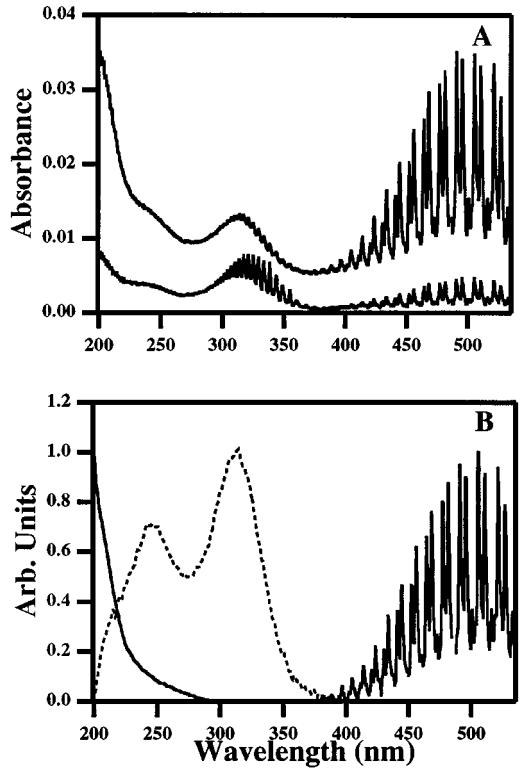

Figure 2. (A) Absorption spectrum of OBrO source with (upper spectrum) and without (lower spectrum) O atom discharge (see text for details). The upper spectrum has been shifted up by 0.005 absorbance units for clarity. (B) spectra of OBrO (solid line) and Br_xO_y (dashed line) obtained from an analysis of spectra recorded over the temperature range 296−333 K with and without the O atom discharge.

its strong absorption at the short wavelengths combined with a weaker absorption between 300 and 350 nm. Br_2O was not observed when the O atom discharge was on. As will be discussed below, the short-wavelength component (discharge on) correlates with the 500 nm OBrO band. Therefore, we have assigned this to OBrO. The continuous absorption feature which shows peaks at 240 and 310 nm is an as yet unidentified molecule(s). We assume in the discussion below that this species is a single molecule and is a bromine oxide, Br_xO_y. We assume Br_xO_y to be one species because over the range of conditions used in this study its absorption spectrum did not change shape. Bromine oxides other than OBrO and Br_2O were not identified in the previous kinetic studies of Li[4,5] and Butkovskaya.[3]

The spectra recorded with the O atom discharge show several important differences. These changes were used to identify the various absorption features and aid in the OBrO absorption cross section determination. First, the OBrO absorption is significantly larger with the O atom discharge. Typically, the OBrO signal increased between a factor of 5−10. Most likely, the O atoms react with the solid sample in the trap to either yield OBrO directly or a gas phase product that readily decomposes to OBrO. Second, the BrO absorption signal is reduced by a factor of 3−5. Third, the Br_xO_y absorption increases very slightly ∼30%. We also found that the temperature of the absorption cell affected the relative intensity of the absorption features. Increasing the temperature from 273 to 333 K resulted in a decrease in the absorption by OBrO and Br_xO_y with an increase in the BrO signal. At the highest temperature used, 333 K, only BrO was detected in the absorption spectrum.

The temperature and O atom dependence of the measured absorption spectra were used to separate the OBrO and Br_xO_y spectra, Figure 2B. OBrO absorbs strongly at the short-wavelength limit of our measurements. This is consistent with the analogous OClO absorption spectrum which has a strong continuous absorption that is about 200 nm below its strong vibrational banded feature.[19] It should be pointed out, however, that the relative intensity of the short-wavelength band to the 500 nm band determined in this work is only accurate to ∼±30%. This uncertainty, however, does not influence the cross section determination of the 500 nm band.

Based on the qualitative observations from the changes in the OBrO, BrO, and Br_xO_y absorption signals with temperature, it appears that the chemical system is in or near equilibrium.

$$Br_xO_y \rightarrow \leftrightarrow \rightarrow BrO + OBrO \qquad (4)$$

The multiple arrows indicate that other unidentified reaction intermediates may be involved. The equilibrium expression

$$K_C = A(BrO)A(OBrO)/A(Br_xO_y) \qquad (5)$$

where the absorption signals are taken at the peak of the 7−0 band for BrO, 710−000 band for OBrO, and at 310 nm for Br_xO_y yields $K_C \sim 1000 \pm 500$ at 296 K. Note that K_C could be a product of equilibrium constants. The value of K_C was found to decrease with increasing temperature to ∼100 at 333 K. This corresponds to a $\Delta_r H°$ value of ∼−13 kcal mol^{-1}, if there is only one reaction involved. If mulitple reactions are involved, it will be the sum of the enthalpy changes for the reactions.

OBrO Absorption Cross Section. The OBrO absorption signal was found to be dependent on the residence time in the absorption cell. The cell residence time was increased by reducing the pumping speed, which also increased the pressure. We observed the OBrO signal to increase as the residence time was increased from 0.1 to 0.2 s. However, still longer residence times showed significant decreases in the OBrO absorption signal. In these measurements, the equilibrium relationship given in eq 5 was maintained for all residence times. Any OBrO concentration profiles along the length of the absorption cell (we measure the column OBrO absorption) need to be accounted for in the cross section analysis.

The OBrO concentration profile along the cell under fast flow conditions was measured by titrating it with NO. NO was added, in large excess, at various distances along the absorption cell. A large NO excess was used because we observed that both OBrO and Br_xO_y (and BrO) were removed when NO_2 was added to the cell. The large NO excess avoided complications from loss of NO_2 due to reactions with other species. Absorption spectra were recorded with and without NO added. The analysis indicated that the concentration gradient at 298 K was small and could be expressed with a first-order loss rate coefficient of 6 ± 1 s^{-1}, i.e. 20% OBrO loss over the length of the cell. The first-order loss rate coefficient for Br_xO_y was $\sim 11 \pm 6$ s^{-1}. We were unable to titrate OBrO without changing the Br_xO_y concentration because of its possible reaction with NO

$$Br_xO_y + NO \rightarrow \text{products} + NO_2 \qquad (6)$$

and/or through reequilibration via reaction 4. In either case, the concentration of measured NO_2 was influenced by Br_xO_y.

Experiments were carried out at several different temperatures in the range 283−343 K in an attempt to alter the relative proportions of OBrO to Br_xO_y. However, at temperatures greater than 303 K, where the proportions would measurably change, both species suffered significant concentration gradients. Therefore, all the titration measurements were limited to room temperature.

In a multicomponent absorption system, the individual absorption spectra could be determined using a set of linear equations provided the components have sufficiently different features and their proportion could be varied. In our system it is difficult to vary the relative proportion because the components are coupled through reaction 4 and under our conditions the Br_xO_y/OBrO ratio could not be widely varied. Our best method to vary the Br_xO_y/OBrO ratio was through the use of the O atom discharge. The NO_2 yield in the titration of this mixture of species is given by

$$[NO_2] = 2[OBrO] + y[Br_xO_y] + [BrO] \quad (7)$$

where the coefficients represent the NO_2 yield from each molecule. The OBrO coefficient is 2 because of the reactions

$$NO + OBrO \rightarrow NO_2 + BrO \quad (1)$$

$$NO + BrO \rightarrow NO_2 + Br \quad (8)$$

which yield two NO_2 molecules for each OBrO molecule. The coefficient for Br_xO_y, y, is not as clearly defined due to the unknown secondary chemistry that may occur. However, we have assumed that for measurements for which $[Br_xO_y]$ are nearly constant, the y coefficient is valid. The BrO contribution to the total NO_2 signal is relatively small. Therefore, for the subsequent analysis we have subtracted its contribution to the $[NO_2]$ to obtain $[NO_2]_{corr}$. Expressing eq 7 in terms of our measured quantities yields

$$[NO_2]_{corr} = 2[A(OBrO)/(L\sigma(OBrO))] + y[A(Br_xO_y)/(L\sigma(Br_xO_y))] \quad (9)$$

where L is the absorption path length. Plotting the quantity $[NO_2]_{corr}L/A(Br_xO_y)$ vs the quantity $A(OBrO)/A(Br_xO_y)$ yields a slope of $2/\sigma(OBrO)$ and an intercept equal to $y/\sigma(Br_xO_y)$.

Fourteen pairs (O atom discharge on and off) of data were used in the final cross section determination. The effective Br_xO_y cross section, $\sigma(Br_xO_y)/y$, obtained from a linear least-squares analysis was $(2.19 \pm 0.80) \times 10^{-18}$ cm^2 molecule^{-1}. The OBrO cross section at the peak of the 710 ← 000 transition was found to be $(1.76 \pm 0.5) \times 10^{-17}$ cm^2 molecule^{-1}. This value includes a 10% correction to account for the OBrO concentration gradient in the absorption cell. The quoted uncertainties are two standard deviations of the slope in the above fit. The OBrO cross section values obtained from each data pair (O atom discharge ON and OFF) are shown in Figure 3, where the asymmetric error bars shown are derived from the uncertainty in the Br_xO_y effective cross section given above. The small range over which the $[OBrO]/[Br_xO_y]$ ratio could be varied led to the significant uncertainty in the OBrO absorption cross section. Experiments with the injector positioned in the middle of the cell yielded similar results but with larger uncertainties due to the reduced path length for both the NO_2 and OBrO absorption measurements. We report in Table 1 the OBrO peak cross section values using the 0.66 nm resolution spectrum shown in Figure 1and the transition assignments reported by Miller et al.[7]

If the contribution of Br_xO_y to the NO_2 signal was ignored, i.e., all the measured NO_2 came from OBrO, a cross section value of $(1.06 \pm 0.4) \times 10^{-17}$ cm^2 molecule^{-1} would be obtained. This represents a lower limit to the OBrO cross section.

The recent OBrO kinetic measurements of Li[4] and Li and Tao[5] did not consider the presence of Br_xO_y in the flow tube. The presence of higher bromine oxides as observed in this work could affect their kinetic measurements in two ways. First, the apparent equilibrium observed in this work, reaction 4, could regenerate OBrO in the flow tube. This would lead to a systematic underestimate of the OBrO loss. Second, the higher bromine oxide might interfere with the mass spectrometric detection of OBrO. It is likely that the higher oxides would fragment onto the OBrO parent peak when using electron impact mass spectrometry. In light of the present observations, a reevaluation of their kinetic results and OBrO detection via mass spectrometry may be warranted.

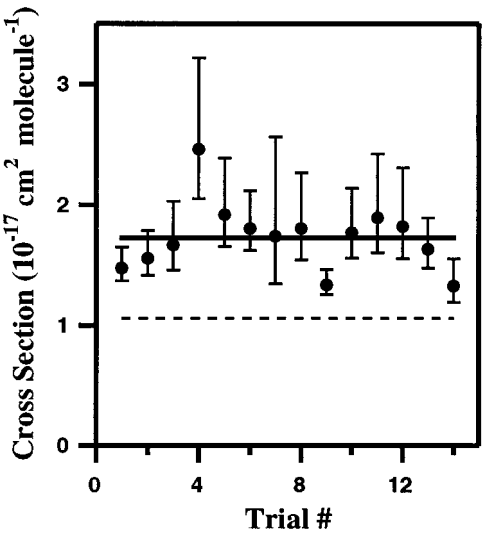

Figure 3. OBrO absorption cross section measurements. The error limits in the individual points are derived from the 2σ uncertainty in the effective Br_xO_y cross section value (see text). The solid line is the average OBrO cross section value, 1.76×10^{-17} cm^2 molecule^{-1}, while the dashed line represents the minimum cross section value, 1.06×10^{-17} cm^2 molecule^{-1}.

TABLE 1: OBrO Absorption Cross Sections (298 K, 0.66 nm Resolution)

n	$(n,0,0) \leftarrow (0,0,0)$ nm	σ^a	$(n,1,0) \leftarrow (0,0,0)$ nm	σ^a
0	630.4		622.0	
1	606.1		598.4	
2	583.8		576.8	
3	563.4	1.08	556.8	1.35
4	544.4	1.45	538.5	1.74
5	527.1	1.64	521.6	1.91
6	510.7	1.77	505.5	1.96
7	495.5	1.72	490.7	1.76
8	481.2	1.67	476.9	1.51
9	468.2	1.44	464.1	1.26
10	455.8	1.21	452.2	0.96
11	444.4	1.02	440.8	0.72
12	433.7	0.79	430.4	0.49
13	423.5	0.57	420.6	0.31
14	414.1	0.40	411.0	0.22
15	405.1	0.26	402.3	0.13
16	396.4		394.0	
17	388.3			

[a] Units: 10^{-17} cm^2 molecule^{-1}.

Characterization of Br_xO_y. The identity of Br_xO_y remains unknown. However, in an effort to characterize the Br_xO_y species, we have recorded UV and IR absorption spectra of the condensed sample to accompany our gas phase UV spectra. Both UV/vis and IR absorption spectra were obtained by condensing material onto a cooled window located in the optical path. Samples were deposited on the cold windows either from the sample trap or by collecting the effluent from the microwave discharge source. The measured spectra are shown in Figure 4.

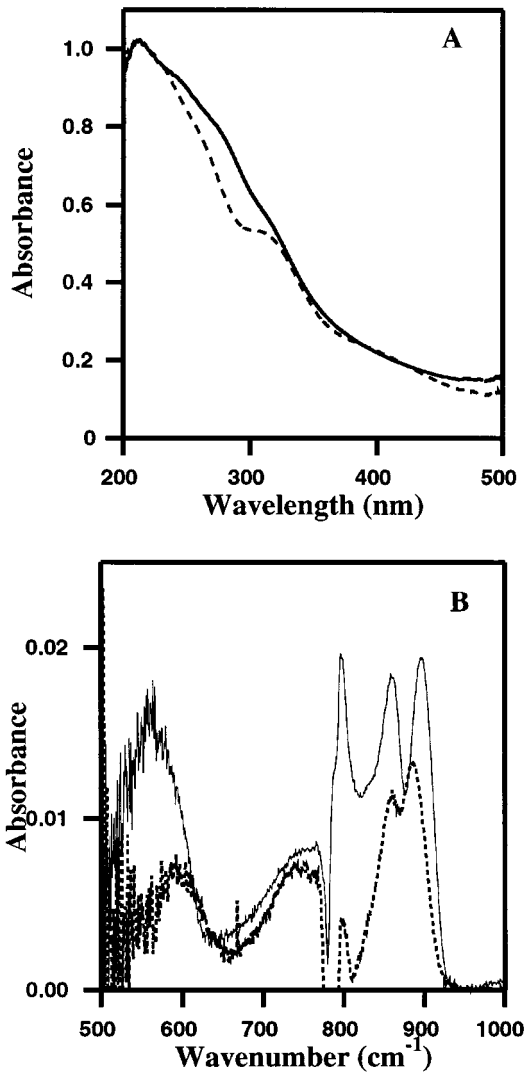

Figure 4. (A) UV absorption spectra of the OBrO source effluent condensed on a quartz window at 230 K (B) IR absorption spectra of the OBrO source effluent (solid line) and the effluent of a Br_2/O_2 microwave discharge condensed on a KBr window (dashed line). The dip observed in the spectrum between 765 and 805 cm^{-1} resulted from an interaction of the sample with the substrate material and remained after warming the window.

OBrO was not observed in either the UV/vis or IR spectra.[7,14,20] The UV/vis spectra show an absorption feature similar to the unidentified (gas phase) bromine oxide, Br_xO_y. The condensed phase spectra obtained with the O atom discharge running showed some differences. IR absorption spectra were recorded using a benchtop interferometer at 1 cm^{-1} resolution with a KBr substrate. The spectra showed a dependence on the method of deposition used. Because of the lack of published spectral data, identification of the absorption bands was not possible. However, bands attributable to OBrO,[7] BrO_3,[21] Br_2O,[22] $(BrO)_2$,[22] or Br_2O_3[23] were not observed.

We have too little information at present to make even a tentative assignment to Br_xO_y. In Chase's review (also see references within) of the bromine oxides, $Br_2O_5(O_2BrOBrO_2)$, $Br_2O_6(O_2BrOBrO_3)$, and $Br_2O_7(O_3BrOBrO_3)$ are all tentatively assigned to white solids whereas the majority of our solid sample, collected at 240 K, was yellow-brown.[24] $Br_2O_3(BrOBrO_2)$ has been identified as a lemon-yellow crystal.[25] It is very likely that our condensed samples contain a mixture of these bromine oxides. Note, however, that there is no guarantee that the sample observed in the solid phase is the same as in the gas phase. Each of these bromine oxides could lead to the formation of OBrO in the gas phase via thermal decomposition or reaction with O atoms. The identification of these bromine oxides in the gas phase would be desirable.

Conclusions

The UV/vis absorption cross sections of OBrO have been measured using a chemical titration method. These values can be directly applied to the interpretation of atmospheric trace gas measurements using occultation techniques. During the course of this work, we have observed a previously unidentified UV absorption spectrum of another bromine oxide, Br_xO_y, coming from the OBrO source.

Acknowledgment. We thank E. R. Lovejoy for helpful discussions. This work was funded in part by the upper atmospheric research program of NASA.

References and Notes

(1) McElroy, M. B.; Salawitch, R. J.; Wofsy, S. C.; Logan, J. A. *Nature* **1986**, *321*, 759.
(2) Solomon, S. *Nature* **1990**, *347*, 347.
(3) Butkovskaya, N. I.; Morozov, I. I.; Tal′rose, V. L.; Vasiliev, E. S. *Chem. Phys.* **1983**, *79*, 21.
(4) Li, Z. *J. Phys. Chem*. A **1999**, *103*, 1206.
(5) Li, Z.; Tao, Z. *Chem. Phys. Lett*. **1999**, *306*, 117.
(6) Rattigan, O. V.; Jones, R. L.; Cox, R. A. *Chem. Phys. Lett*. **1994**, *230*, 121.
(7) Miller, C. E.; Nickolaisen, S. L.; Francisco, J. S.; Sander, S. P. *J. Chem. Phys*. **1997**, *107*, 2300.
(8) Rowley, D. M.; Harwood, M. H.; Freshwater, R. A.; Jones, R. L. *J. Phys. Chem*. **1996**, *100*, 3020.
(9) Burkholder, J. B. *Int. J. Chem. Kinet*. **1998**, *30*, 571.
(10) Orlando, J. J.; Burkholder, J. B. *J. Phys. Chem*. **2000**, *104*, 2048.
(11) Renard, J. B.; Pirre, M.; Robert, C.; Huguenin, D. C. *J. Geophys. Res*. **1998**, *103*, 25383.
(12) Chipperfield, M. P.; Glassup, T.; Pundt, I.; Rattigan, O. V. *Geophys. Res. Lett*. **1998**, *25*, 3575.
(13) Erle, F.; Platt, U.; Pfeilsticker, K. *Geophys. Res. Lett*. **2000**, *27*, 2217.
(14) Kolm, J.; Engdahl, A.; Schrems, O.; Nelander, B. *Chem. Phys*. **1997**, *214*, 313.
(15) Muller, H. S.; Miller, C. E.; Cohen, E. A. *J. Chem. Phys*. **1997**, *107*, 8292.
(16) Maric, D.; Burrows, J. P.; Moortgat, G. K. *J. Photochem. Photobiol. A* **1994**, *83*, 179.
(17) DeMore, W. B.; Sander, S. P.; Golden, D. M.; Hampson, R. F.; Kurylo, M. J.; Howard, C. J.; Ravishankara, A. R.; Kolb, C. E.; Molina, M. J. "Chemical Kinetics and Photochemical Data for Use in Stratospheric Modeling"; Eval. 12. JPL, 1997.
(18) Gierczak, T.; Burkholder, J. B.; Ravishankara, A. R. *J. Phys. Chem*. **1999**, *103*, 877.
(19) Hubinger, S.; Nee, J. B. *Chem. Phys*. **1994**, *181*, 247.
(20) Pacios, L. F.; Gómez, P. C. *J. Phys. Chem*. **1997**, *101*, 1767.
(21) Pacios, L. F.; Gómez, P. C. *Chem. Phys. Lett*. **1998**, *289*, 412.
(22) Kölm, J.; Schrems, O.; Beichert, P. *J. Phys. Chem*. **1998**, *102*, 1083.
(23) Guha, S.; Francisco, J. S. *J. Phys. Chem*. **1998**, *102*, 6702.
(24) Chase, M. W. *J. Phys. Chem. Ref. Data* **1996**, *25*, 1069.
(25) Kuschel, R.; Seppelt, K. *Angew. Chem., Int. Ed. Engl*. **1993**, *32*, 1632.